THE JOURNAL OF PHYSICAL CHEMISTRY A

Article

pubs.acs.org/JPCA

Valence Shell Photoelectron Spectroscopy of Pyrene and Fluorene: Photon Energy Dependence in the Far-Ultraviolet Region

Preeti Manjari Mishra,[†] Lorenzo Avaldi,[‡] Paola Bolognesi,[‡] Kevin C. Prince,[§,∥,⊥] Robert Richter,[§] and Umesh R. Kadhane*[,†]

[†]Indian Institute of Space Science and Technology, Thiruvananthapuram 695547, Kerala, India

[‡]CNR-Istituto di Metodologie Inorganiche e dei Plasmi, Area della Ricerca di Roma 1, CP10-00016 Monterotondo, Italy

[§]Elettra-Sincrotrone Trieste, Strada Statale 14, km 163.5, Area Science Park, I-34149 Basovizza, Italy

[∥]Chemistry Laboratory, Faculty of Life and Social Sciences, Swinburne University of Technology, Melbourne, Victoria 3122, Australia

[⊥]Istituto Officina dei Materiali, Consiglio Nazionale delle Ricerche, Area Science Park, I-34149 Trieste, Italy

ABSTRACT: Inner and outer valence photoelectron spectra (PES) of pyrene and fluorene, two members of the polycyclic aromatic hydrocarbon (PAH) family, were recorded with a high-resolution synchrotron photoelectron spectrometer. Relative photoelectron emission cross sections were measured at photon energies between 15 and 40 eV. Several bands observed in the experimental PES were assigned with the help of OVGF/cc-pVDZ calculations. The first ionization potentials were estimated to be 7.436 ± 0.015 and 7.944 ± 0.055 eV for pyrene and fluorene, respectively. Photoelectron emission cross sections show a clear difference in trend for inner (σ-dominated) and outer (π-dominated) bands. Contrary to the expectation from the trend observed in benzene, the inner bands significantly dominate in the photon energy region from 15 to 27 eV and then are found to contribute uniformly. A pronounced peak in the cross sections is observed at a photon energy of approximately 17 eV for both molecules (irrespective of the difference in symmetry and structure), particularly for the inner valence bands. The feature is observed to be independent of the details of the molecular orbital associated with the outgoing electron. These observations are correlated to a collective excitation in the far-ultraviolet region.

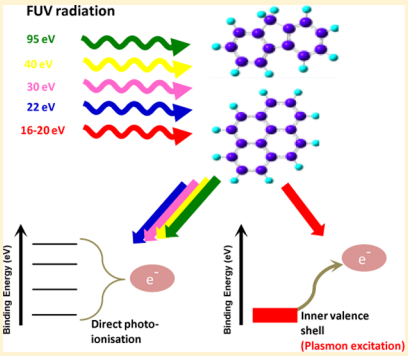

INTRODUCTION

The polycyclic aromatic hydrocarbons (PAHs), molecules formed by fused aromatic rings, are significant components of the terrestrial environment as well as of the interstellar medium (ISM), with a large fraction of interstellar carbon contained in them. PAHs, hydrogenated PAHs, and their radical ions are possible carriers of diffuse interstellar bands and play a vital role in the thermodynamics of the ISM.[1,2] The infrared (IR) spectrum of most stellar objects, ranging from single HII regions and reflection nebulae to galactic nuclei and sometimes entire galaxies, is characterized by broad infrared emission features that resemble the spectroscopic signature of PAHs.[3] These molecules are efficient absorbers of ultraviolet (UV) radiation, particularly because of their $\pi-\pi^*$ transitions in the UV region, coupling electronic energy to vibrational energy and resulting in IR photon emission. They thus contribute to interstellar UV opacity.[4,5] The IR spectra show strong emission features at 3.3, 6.2, 7.7, and 11.3 μm, which have been attributed to PAHs.[3] The radical cation of pyrene is thought to be responsible for major UV−visible interstellar absorption bands.[6−9] Fluorene is also studied as a possible carrier for spectra of electromagnetic radiation from the ISM in terms of the extinction coefficient.[10]

On Earth, PAHs are naturally present in crude oil and coal deposits, arise from chemical conversion of organic molecules, and are also formed by incomplete combustion of carbon-containing fuels. Some PAHs are known to be mutagenic, carcinogenic, or teratogenic environmental pollutants and are found in vehicular exhaust, industrial waste, cigarette smoke, etc.[11] Human contamination by PAHs is mainly through skin absorption, inhalation, or food consumption. Because they contain multiple aromatic ring systems, these compounds can absorb light in the UV-A (320−400 nm) or visible region (400−700 nm),[2] forming reactive species and causing damage to human metabolism along with DNA cleavage.[12,13] Therefore, a detailed understanding of the photochemistry of PAHs is needed to determine the relationship among the photo-mutagenicity, photostability, and structure of PAHs. Fluorene and multilayered polymers of fluorene (polyfluorenes), moreover, are particularly interesting systems for nanoelectronics, optoelectronics, and organic LEDs.[14]

A typical photoabsorption spectrum of a PAH in the visible, UV, and far-UV regions is characterized by various molecular excitations starting from the outermost $\pi-\pi^*$ excitations to the inner ones like $\pi-\sigma^*$, $\sigma-\pi^*$, and $\sigma-\sigma^*$ excitations. The positions and oscillator strengths of the $\pi-\pi^*$ transitions for

Received: March 11, 2014
Revised: April 2, 2014
Published: April 7, 2014

   dx.doi.org/10.1021/jp502445d | J. Phys. Chem. A 2014, 118, 3128−3135

different PAHs vary because of the difference in symmetry and molecular structure, but a very prominent broad feature at approximately 17 eV is commonly observed in all PAHs.[15,16] This feature can be attributed to collective or plasmon excitation as well as a mixture of various inner shell transitions like $\sigma-\pi^*$, $\pi-\sigma^*$, and $\sigma-\sigma^*$ transitions. Similar features observed in the case of graphite and graphene have been explained by Drude's model for electronic structure. In the case of C_{60}, an analogous feature appears at ∼21 eV, close to that observed in graphite at ∼25 eV.[16] Considering the two-dimensional structure of PAHs, this feature should be expected at ∼17 eV[16] and has been observed in electron energy loss spectroscopy studies of PAH films and photo ion yield studies in the gas phase.[16] State selective photoemission intensities as a function of photon energy have never been measured for PAHs except benzene. Jochims et al.[16] have studied the photo ion yield of several PAHs in the far-UV region and observed that in spite of a substantial variation in the ionization potentials, the ion yield for a single ionization almost always peaks at 17 eV.

Photoelectron spectroscopy of PAHs was conducted mainly with He I and He II discharge sources[17−19] in the 1970s. Theoretical investigations, including the most recent ones,[20] rely substantially on these old measurements. In the study presented here, synchrotron radiation has been used to investigate the systematic variation of the state selective photoelectron cross sections over a wide range of photon energies.

The prominent peaks in the photoelectron spectrum (PES) are identified according to their binding energy and symmetry with the help of outer valence Green's function (OVGF) calculations. To a first approximation, each peak in PES can be attributed to a molecular orbital at least in the outer valence region. This type of analysis helps in understanding the electronic and bonding properties of the molecule. The PES of a molecule is typically associated with a broadening due to Franck−Condon overlap of vibrational states. The inner valence bands are characterized by satellite peaks due to configuration interaction between quasi degenerate states with a single hole configuration in inner valence band and states with a configuration with two holes in an outer valence band along with one particle in an excited orbital. This strong interaction due to electron−electron correlation leads to the redistribution of intensity over several satellite lines, which is a manifestation of the breaking down of the molecular orbital picture of ionization.[21−24] Advanced calculations that take care of the electron−electron correlation as well as of the relaxation energy correction to represent the PES peak positions with a reasonable accuracy include configuration interaction techniques, perturbation techniques, and Green's function methods.[25] For a reliable calculation of ionization energies and their relative intensities (pole strength), it is necessary to describe as accurately as possible the many-body effects that are very important in photoelectron spectra. For this work, we have used the Green's function technique implemented in GAUSSIAN 09.

EXPERIMENTAL DETAILS

The experiment was performed at the GASPHASE photoemission beamline at the Elettra-Sincrotrone Trieste laboratory (Trieste, Italy). The layout of the beamline and details of the experimental station have been described previously.[26] The typical resolving power of the beamline is 2000 at the energies used here. A hemispherical electron energy analyzer with six-channel electron multiplier detectors was used to measure the photoelectron spectra with a resolution down to 50 meV. The spectrometer acceptance angle is a cone of ±4° with the axis of the cone oriented at the magic angle with respect to the direction of polarization.

The photon beam crosses an effusive beam of the target molecules. Pyrene and fluorene were obtained from Sigma-Aldrich at >99% purity. The target was placed in a copper container having a 3.3 cm length nozzle with a 3 mm opening. The container for pyrene was heated resistively to ∼74 °C, which was kept constant with the help of a temperature controller. A time-of-flight spectrum taken from the same measurement (not shown here) showed no trace of impurity or fragment peaks, so dissociation of the molecule from heating was insignificant. For fluorene, the vapor pressure was sufficiently high to avoid any heating. The photoelectron spectra were recorded for a wide range of photon energies from 15 to 40 eV. In the case of pyrene, a data set at 95.1 eV also has been recorded. Xenon flow was adjusted to maintain a constant chamber pressure while the full set of data for Xe was acquired.

Normalization Procedure for Estimation of Relative Cross Sections from PES. The intensity of the photon beam was measured with a photodiode whose efficiency increases with photon energy. However, because of the larger harmonic contribution at a lower photon energy, a direct normalization of the data to the photodiode current was not possible. Therefore, the measurements of the xenon ionization cross section were used to obtain the normalization to the photon flux. To extract the correct factor, the beam conditions at a given photon energy (i.e., entrance and exit slits, undulator gap, etc.) were kept identical for all three targets, namely, xenon, pyrene, and fluorene. Xenon photoelectron peak areas measured in this study were compared with the previously published absolute cross sections for Xe *5p* photoionization.[27,28] This procedure was followed over the whole photon energy range that was studied. The normalization factors obtained were used for normalizing the area obtained for pyrene and fluorene. Xe Auger electron spectra were also recorded at a photon energy of 95.1 eV to obtain the transmission function of the spectrometer by comparing the Auger intensity distribution reported in previous investigations.[29] The efficiency curve was obtained by fitting a polynomial to the measured factors for each individual channel electron multiplier. The relative photoelectron cross sections were finally obtained by including photon flux normalization and spectrometer efficiency correction (assuming a constant target density). These relative cross sections are directly proportional to the absolute cross sections, by a constant factor unique to each target molecule.

COMPUTATIONAL DETAILS

The ground-state geometries of pyrene and fluorene were optimized with the constraint of D_{2h} and C_{2v} symmetry point groups,[30] respectively, using density functional theory (DFT).[31−33] We employed the nonlocal hybrid Becke three-parameter Lee−Yang−Parr functional (B3LYP)[34,35] and Dunning's correlation consistent polarized valence basis set of double-ζ quality (cc-pVDZ),[36,37] incorporated in the GAUSSIAN 09 package for these calculations.[38] OVGF calculations were conducted using Dunning basis set cc-pVDZ to predict molecular orbital ionization energies with respective pole strengths. We include all the orbitals in the calculation, and the calculations are restricted to ionization potentials of <20 eV.[38]

dx.doi.org/10.1021/jp502445d | J. Phys. Chem. A 2014, 118, 3128−3135

RESULTS AND DISCUSSION

Experimental and Calculated PES for Pyrene. The measured PES in the inner and outer valence region of pyrene at a photon energy of 27 eV is presented in Figure 1a, with the

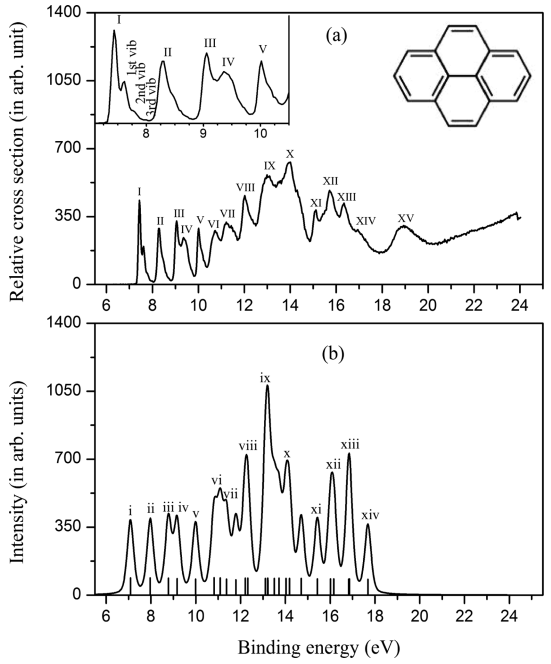

Figure 1. (a) Experimental PES of pyrene at a photon energy of 27 eV (outer valence band details in the inset). (b) OVGF calculations convoluted with a 0.3 eV width Lorentzian and Gaussian (—). The bar graph shows the pole strength for a given binding energy peak.

dominant peaks labeled with Roman numerals. For the sake of convenience, uppercase Roman numerals are used while discussing experimental bands and lowercase Roman numerals in the context of theoretical bands. Figure 1b shows the convoluted spectrum from the OVGF/cc-pVDZ calculations. A sum of Gaussian and Lorentzian functions with 0.3 eV widths is used for the convolution. Orbital symmetry assignments are made by comparing the binding energies of experimental and theoretical peaks obtained by OVGF calculations that are listed in Table 1. The first ionization energy is found to be 7.436 ± 0.015 eV (I), which compares very well with the values obtained with REMPI-ZEKE and TPEPICO of 7.426 and 7.415 eV, respectively.[39] This HOMO band is accompanied by its vibrational progression that can be resolved up to 3 ← 0 transitions. This is followed by a well-isolated II band at 8.30 eV. The III and IV bands are observed to overlap and, according to the OVGF calculations, originate from the π MOs b_{3u} (band iii) and a_u (band iv). Band IV shows a much broader structure, indicating possible coupling to other states leading to breakdown of the MO picture as described by Deleuze et al.[20] Band V retains the sharp distribution with a poorly resolved vibrational substructure at 10.01 eV. The corresponding peak appears at 9.99 eV according to the OVGF calculations. The outer valence binding energies up to band V match with the OVGF calculations within 0.40 eV (see Table 1).

From band VI onward, the individual MOs are very close in energy, leading to a strong overlap of the bands. This scenario is made worse by the fact that strong electron−electron correlation effects lead to the mixing of several configurations with the redistribution of the intensity of the individual bands.

Table 1. Molecular Orbital Calculations for Pyrene with OVGF Estimates of Binding Energy and Pole Strength Using the cc-pVDZ Basis Set in Comparison with the Experimentally Measured Binding Energy[a]

MO	type	Koopman theorem value (eV)	OVGF (eV)	pole strength	label used in Figure 1	experimental binding energy (eV)
$2b_{1g}$	π	7.03	7.08	0.89	I	7.43
$2b_{2g}$	π	8.07	7.97	0.88	II	8.30
$3b_{3u}$	π	9.36	8.78	0.88	III	9.05
$1a_u$	π	9.86	9.17	0.86	IV	9.38
$2b_{3u}$	π	10.97	9.99	0.83	V	10.01
$9b_{3g}$	σ	12.57	10.82	0.89	VI	10.73
$1b_{1g}$	π	12.62	11.38	0.83		
$14a_g$	σ	12.92	11.09	0.89		
$1b_{2g}$	π	13.40	11.79	0.79	VII	11.21
$10b_{2u}$	σ	14.09	12.21	0.88	VIII	12.02
$12b_{1u}$	σ	14.14	12.32	0.88		
$8b_{3g}$	σ	14.91	13.10	0.87	IX	13.01
$1b_{3u}$	π	15.16	13.23	0.76		
$11b_{1u}$	σ	15.18	13.21	0.88		
$9b_{2u}$	σ	15.32	13.50	0.87		
$13a_g$	σ	15.81	13.72	0.87		
$8b_{2u}$	σ	16.34	14.18	0.86	X	13.94
$7b_{3g}$	σ	16.39	14.03	0.86		
$12a_g$	σ	16.64	14.71	0.86		
$10b_{1u}$	σ	17.55	15.43	0.85	XI	15.11
$11a_g$	σ	18.39	16.01	0.84	XII	15.74
$7b_{2u}$	σ	18.68	16.17	0.84		
$10a_g$	σ	19.29	16.83	0.83	XIII	16.34
$6b_{3g}$	σ	19.37	16.86	0.84		
$9b_{1u}$	σ	20.42	17.69	0.82	XIV	16.94

[a]Uppercase Roman numerals are used to label experimental bands and lowercase Roman numerals for theoretical bands.

This leads to severe broadening of the peak structure. Bands starting from VI to X mix very strongly, and the OVGF results qualitatively match the peak positions of bands VIII−X. Bands above and including band XI appear to be well separated and again match closely the calculated band positions.

Experimental and Calculated PES for Fluorene. The PES for fluorene at a photon energy of 27 eV is presented in panels a and b of Figure 2. The assignment of the inner and outer valence molecular orbital has been made by comparing the theoretical binding energies [obtained from OVGF calculations (see Table 2)] with the measured PES binding energy. Figure 2 shows qualitative agreement in energy as well as in intensity between theory and experimental PES. To the best of our knowledge, the theoretical fluorene PES spectrum has not yet been reported at this level of calculation. In Figure 2a, the outermost ionization line at 7.944 eV (I) originates from a π MO that is placed at 7.66 eV (i) by OVGF calculations. This peak is associated with poorly resolved vibrational transitions. The vibrational structure for fluorene is more complex because its symmetry is lower than that of pyrene where the bands are clearly resolved.

The well-resolved lines at 8.80 eV (IIa) and 9.10 eV (IIb) compare well with the calculated band ii formed by two closely spaced MOs at 8.48 and 8.71 eV. Both MOs contribute with the same intensity in the experimental and theoretical PES. Band III at 9.85 eV matches well with the calculated band iii at 9.64 eV. This band is also accompanied by its vibrational progression. Band IV and the following bands are well

dx.doi.org/10.1021/jp502445d | J. Phys. Chem. A 2014, 118, 3128−3135

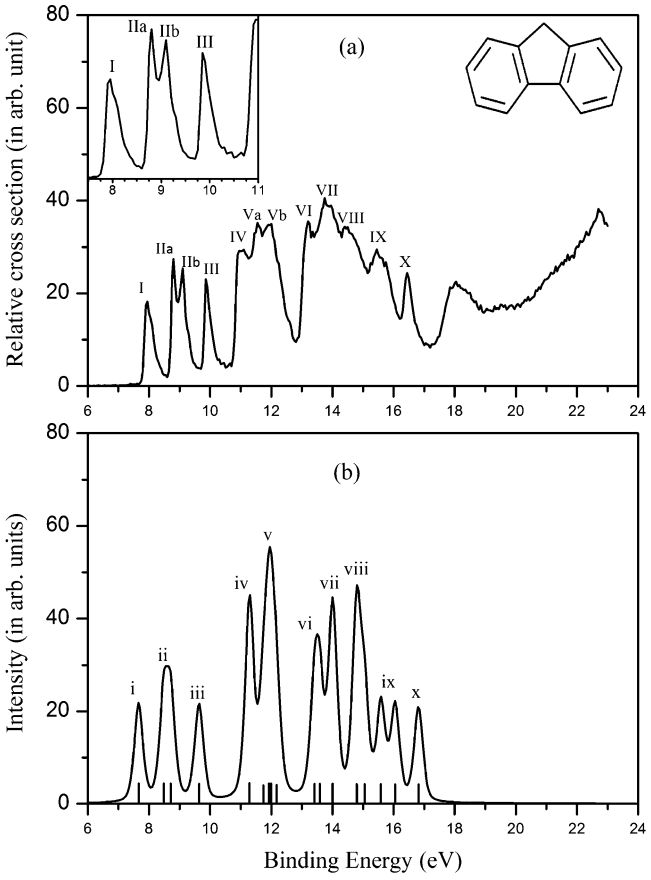

Figure 2. (a) Experimental PES of fluorene at a photon energy of 27 eV (outer valence band details in the inset). (b) OVGF calculations convoluted with a 0.3 eV width Lorentzian and Gaussian (—). The bar graph shows the pole strength for a given binding energy peak.

separated from band III. Band IV in PES can be attributed to a pair of MOs with almost identical binding energy originating from a_1 at 11.29 eV and b_2 at 11.28 eV (see Table 2). Band V shows a complex substructure that can be attributed to the overlap of four MOs (v) as per OVGF with possible distortions due to shake-up processes. Bands VI–VIII appear to dominate the region experimentally as well as theoretically. Finally, bands IX and X come fairly close to the calculated values and also reproduce relative intensities with respect to preceding bands. Overall, the structure observed experimentally is well reproduced as for the valence bands, and the calculated band positions can be reliably associated with the measured positions.

In summary, the outer valence region of our experimental PES for both pyrene and fluorene is reproduced in terms of binding energy within 0.4 eV or better with the present OVGF calculations at the cc-pVDZ level. The overall agreement between experimental and theoretical binding energy can be improved by extending the basis set in the calculations.[40−42] The difference due to the basis set is estimated to be approximately 1−2% by the comparison with the calculations conducted by Mayer et al. at the cc-pVTZ level.[39]

Evolution of the PES with Photon Energy. Relative photoelectron cross sections are plotted as a function of photoelectron binding energy and photon energy in Figures 3 and 4 for pyrene and fluorene, respectively. The measured cross sections for a given target molecule are proportional to the absolute cross section within a constant factor independent of

Table 2. Molecular Orbital Calculations for Fluorene with OVGF Estimates of Binding Energy and Pole Strength Using the cc-pVDZ Basis Set in Comparison with the Experimentally Measured Binding Energy[a]

MO	type	Koopman theorem value (eV)	OVGF (eV)	pole strength	label used in Figure 2	experimental binding energy (eV)
$3a_2$	π	7.73	7.66	0.89	I	7.94
$4b_1$	π	8.85	8.48	0.89	II	8.80 (IIa)
$2a_2$	π	9.13	8.71	0.88		9.10 (IIb)
$3b_1$	π	10.23	9.64	0.88	III	9.85
$20a_1$	σ	12.89	11.29	0.90	IV	11.05
$17b_2$	σ	12.90	11.28	0.90		
$1a_2$	π	13.21	11.74	0.81	V	11.55 (Va)
$19a_1$	σ	13.60	11.92	0.89		
$16b_2$	σ	13.62	12.17	0.82		11.95 (Vb)
$2b_1$	π	13.68	11.99	0.89		
$18a_1$	σ	15.12	13.41	0.88	VI	13.20
$15b_2$	σ	15.41	13.58	0.88		
$17a_1$	σ	15.86	14.01	0.87	VII	13.75
$14b_2$	σ	16.12	14.00	0.87		
$1b_1$	π	16.39	14.80	0.84	VIII	14.45
$13b_2$	σ	16.59	14.79	0.87		
$16a_1$	σ	17.03	15.05	0.86		
$15a_1$	σ	17.84	15.59	0.86	IX	15.45
$12b_2$	σ	18.16	16.05	0.85		
$14a_1$	σ	19.01	16.82	0.85	X	16.45

[a]Uppercase Roman numerals are used to label experimental bands and lowercase Roman numerals for theoretical bands.

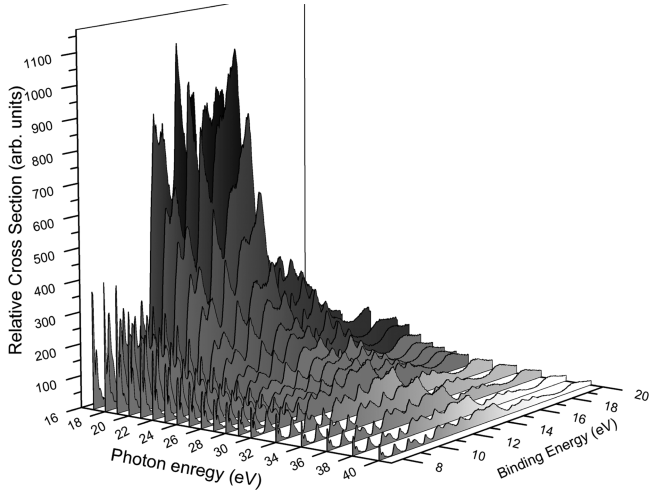

Figure 3. Pyrene photoelectron spectra for different photon energies.

binding energy and photon energy. The figures describe the systematic variation of the various bands as a function of photon energy. They also show a pronounced intensity of the inner valence region at a photon energy of <27 eV.

Above this energy, all the features in the PES evolve in a more uniform manner. The difference in the five outer valence bands for pyrene (three outer valence bands in fluorene) and the inner valence bands is very clear in the photon energy region below 27 eV. One prominent observation is the uniform variation of the cross section above a photon energy of 27 eV. This observation is discussed in more detail later.

The relative intensities (see Figures 5a and 6a) for the outer valence π molecular orbitals as a function of photon energy

dx.doi.org/10.1021/jp502445d | J. Phys. Chem. A 2014, 118, 3128−3135

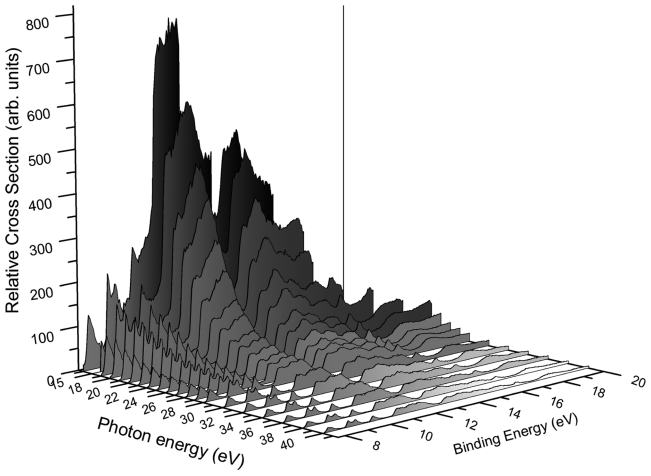

Figure 4. Fluorene photoelectron spectra for different photon energies.

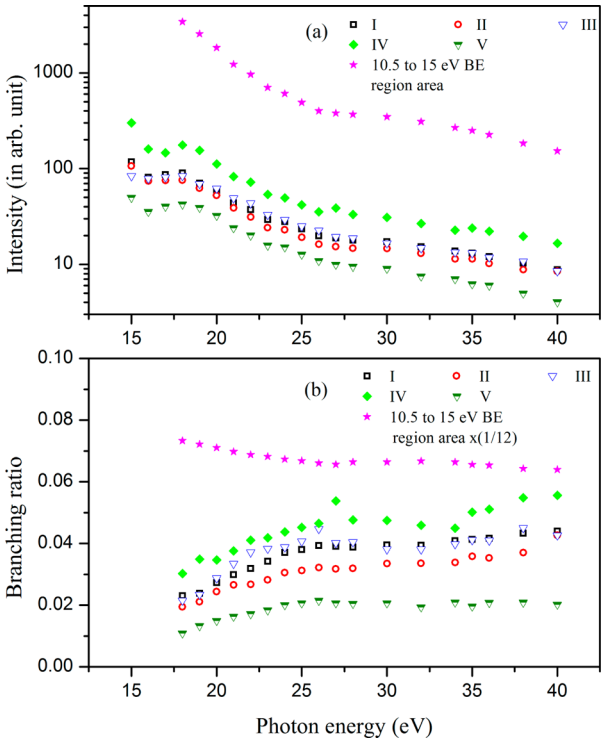

Figure 5. (a) Integrated intensity and (b) branching ratio for various bands of pyrene.

were obtained by determining the area under the peak after background subtraction. For the areas under peaks corresponding to bands III and IV in pyrene (IIa and IIb in fluorene), asymmetric Lorentzian peak fits along with a first-order polynomial for incorporating background subtraction were used. Because the confidence level for the separate fits of bands IIa and IIb in the case of fluorene was not satisfactory, for these bands we report the sum of the intensities. For peaks III and IV in pyrene, the fits were satisfactory, so they are reported separately. For the broad feature (10.50−15.00 and 10.70−12.97 eV binding energy regions in PES for pyrene and fluorene, respectively) resulting from a severe mixing of π and σ MOs, the relative cross sections were obtained without any background subtraction. The branching ratios for the various

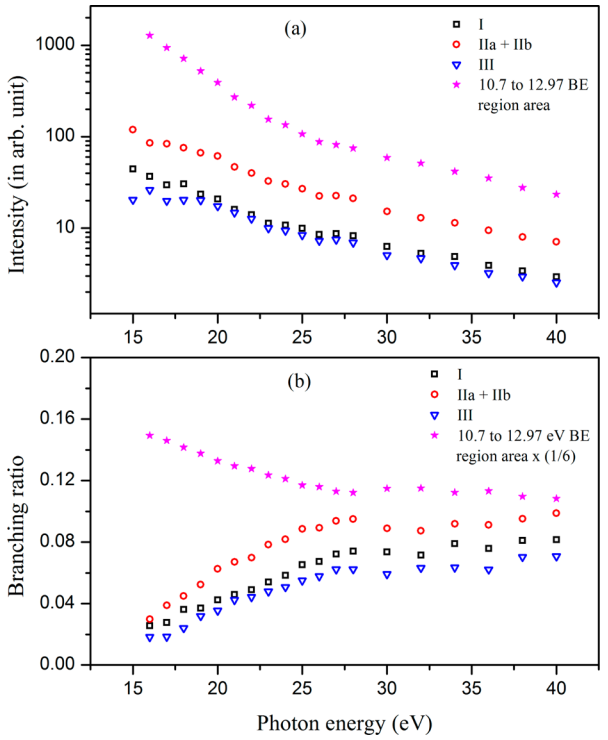

Figure 6. (a) Integrated intensity and (b) branching ratio for various bands of fluorene.

bands shown in Figures 5b and 6b were obtained by taking the ratio of the individual to total PES intensity.

Figure 7 shows the PES scaled with respect to the HOMO intensity for the sake of comparison. A clear observation is that the first five (three) bands in pyrene (fluorene) overlap almost

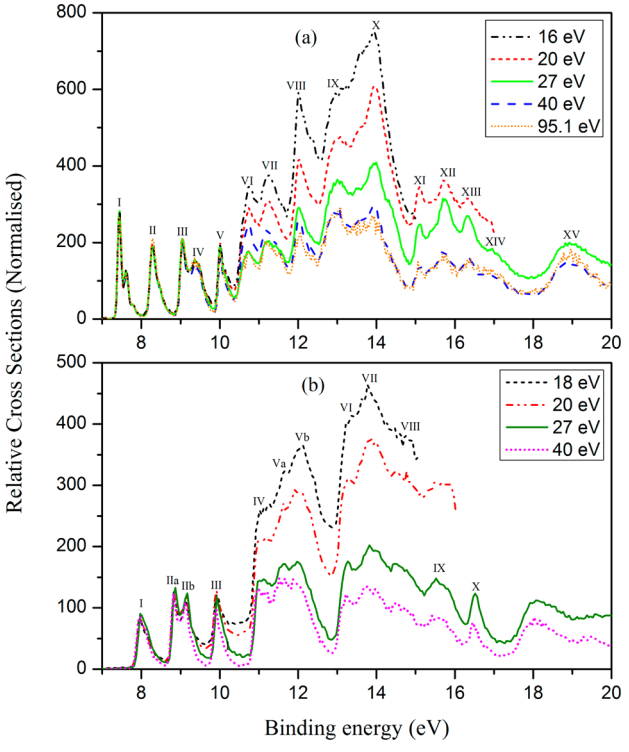

Figure 7. (a) Pyrene and (b) fluorene PES at different photon energies scaled to the intensity of the HOMO band.

dx.doi.org/10.1021/jp502445d | J. Phys. Chem. A 2014, 118, 3128−3135

exactly over the entire photon energy range; however, the inner valence bands show more drastic variation in the lower-photon energy region, while past 27 eV the evolution follows the same trend observed for the renormalized outer valence bands.

Pyrene. Integrated intensities of individual outer valence bands (see Figure 5a) show a similar behavior over the entire photon energy range. All the bands show a peak at ∼17 eV. This parallel trend for the outer π orbital was theoretically predicted for the case of large polyene molecules by Carravetta et al.,[43] but calculations of the dynamics of the photoionization of PAHs have not been performed thus far. In the absence of individual peak fits for the heavily overlapping bands in the inner valence region, it is not possible to separate the individual trends. The overall shape is seen to evolve in the same way for the constituent bands, but there are a few bands within the inner valence region that show a slight variation in the cross section with respect to the nearby bands. It is observed that bands VIII−X contribute strongly to the PES in the 16−27 eV photon energy range. These observations show no direct correlation with either π or σ characteristics of the MO.

PES with five different photon energies are plotted in Figure 7a by scaling the data to the intensity of the HOMO band. The first five bands clearly show almost exact overlap. As Carravetta et al.[43] have shown theoretically, the π orbital photoelectron cross sections evolve similarly. On the other hand, in the case of benzene,[44] particularly at a lower photon energy the individual π MO cross sections show a different trend. Also noteworthy is the almost exact overlap of the full PES for 40 and 95.1 eV photon energy data. Only a small deviation is observed in bands VI and VII.

Fluorene. Despite the fundamental differences in the structure of the two molecules, such as symmetry, the presence of sp^3-hybridized carbon and cyclopentane ring, etc., the photon energy dependences are markedly similar. Figure 4 shows the evolution of PES of fluorene with photon energy. The outer four bands are seen to vary slowly compared to the inner valence bands as seen in the case of pyrene.

The areas under peaks I−III are plotted along with the integrated area of the region from 10.50 to 12.97 eV in Figure 6a. The relative intensities follow the same trend as seen in the case of pyrene. The outer bands display a plateau at ∼17 eV irrespective of the type of MO involved. For the inner band, the peak appears to be at a lower photon energy than for the outer bands, though the exact position cannot be determined within the precision of the present measurements. The relative intensities follow the same trend beyond 27 eV for all the bands. The branching ratios (see Figure 6b) show a behavior similar to that of pyrene. The outer bands contribute less in the lower photon energy than the inner ones up to 27 eV. Beyond that energy, the contributions stabilize and remain uniform up to the end of the photon energy range studied.

The scaled PES in Figure 7b show that in contrast to the outer valence bands that overlap at all photon energies, the inner valence bands show a rapid variation in spite of the scaling to HOMO intensity. Unlike the case for pyrene in which the rapid variation was observed only in the middle of the inner valence region by bands (VIII−X), for fluorene this behavior is observed over the entire inner valence band, from band IV onward. As a function of increasing photon energy, the contribution from band V is seen to decrease faster than that of band IV, whereas in band V itself, that of band Vb decreases more rapidly than that of band Va. Among bands V, VII, and VIII, band VII shows a faster decrease.

Relative Photoionization Cross Section and Branching Ratio as a Function of Photon Energy. The similarity of the behavior of the PES data for pyrene and fluorene indicates that the evolution of photoelectron cross sections is determined by similar processes. The enhancement of the photoionization cross section at a photon energy of ∼17 eV can be explained in terms of a plasmonlike peak resulting from a collective excitation of the valence electrons as already established for C_{60}[45,46] using synchrotron radiation[47] and electron energy loss.[48] The valence electrons in PAH are delocalized and therefore can have collective resonances similar to those of plasmon excitations observed in metal particles.[46,47] This involves oscillator strengths greater than those for the single-electron excitations.[49] The most distinct characteristic we observe is the peak of cross sections at ∼17 eV particularly for the outer valence bands of pyrene (a plateau in the case of fluorene). The increase in inner valence band intensity indicates the proximity of a peak in the absorption cross section but does not show the exact energy of occurrence. This observation is in disagreement with a similar study of benzene by Baltzer et al. and Carlson et al.[44,50] Because the molecules presented here are larger than benzene, it is expected that autoionization processes play a more important role in the far-UV region for pyrene and fluorene than for benzene. It is known that the broad excitation region in PAHs is associated with plasmonlike excitations.[15] This excitation would then couple to various ionization channels. Thus, the ionization cross section from a particular MO is due to the overall variation of the collective excitation cross section. The branching ratios shown in Figures 5b and 6b also demonstrate the dominance of ionization from σ orbitals in the lower-photon energy range, which decreases systematically up to 27 eV and remains constant afterward. This is in contrast with the measurements for benzene[44] where the contribution from σ orbitals systematically grows with photon energy. Baltzer et al.[44] have demonstrated that the inner valence bands contribute more with an increasing photon energy, whereas for pyrene and fluorene, we observe the opposite behavior in the studied photon energy range.

Normally, an excitation of collective nature occurs well above the ionization threshold and is expected to couple to various ionization channels.[44] Because this coupling will be weakly dependent on the photon energy, it is expected that the branching ratio of the photoelectron intensities from various MOs will be constant. The other notable behavior is that in the region of the plasmon excitation the branching ratios of the outer valence bands are lower than those due to the inner valence and shake-up bands. Beyond the plasmon excitation region, the behavior is the same for both inner and outer bands, and they quantitatively display the same trend. This indicates that the plasmon excitation couples more efficiently to the inner valence states.[15,16] It was also shown for coronene that the photoionization cross section at 17.4 eV is primarily due to a giant resonance associated with σ and π electron plasmon excitation.[51] This explanation of a signature of plasmon resonance in both pyrene and fluorene cross sections for a certain range of photon excitation needs improved theoretical modeling.

CONCLUSION

A multidimensional observation of the photoionization cross section of pyrene and fluorene using both the binding energy and the photon energy as variables is presented. The conventional understanding of the molecular photoionization

heavily relies on the binding energy value alone. Here we have studied the photon energy dependence of the relative intensity that sheds light on the details of the inner valence structure of PAHs.

The OVGF method used in the calculation provided binding energy values that compare well with the experimental values, particularly in the energy range where the bands are free from shake-up or shake-off effects. The agreement in most cases was better than 0.40 eV. With the help of these calculations, MO band assignments were made for both molecules.

The photon energy dependence of the relative cross sections was also probed. The evolution of the bands was plotted against photon energy. It was observed that the inner valence bands dominate in the lower-photon energy range (below 27 eV). This is in contrast with the observations made with benzene. The cross sections for the outer valence orbital display a peak for pyrene and a plateau for fluorene at a photon energy of 17 eV. This observation, along with the previously studied photo ion yield studies and EELS studies, indicates that a collective excitation is responsible for this enhancement of the relative cross section. Thus, the observations were explained in terms of a plasmon excitation that couples with various ionization channels during photoexcitation.

AUTHOR INFORMATION

Corresponding Author

*E-mail: umeshk@iist.ac.in. Telephone: 0471-2568550. Fax: 0471-2568542.

Notes

The authors declare no competing financial interest.

REFERENCES

(1) Salama, F.; Bakes, E. L. O.; Allamandola, L. J.; Tielens, A. G. G. M. Assessment of Polycyclic Aromatic Hydrocarbon-Diffuse Interstellar band proposal. *Astrophys. J.* **1996**, *458*, 621−636.

(2) Dabestani, R.; Ivanov, I. N. A compilation of physical, spectroscopic and photophysical properties of polycyclic aromatic hydrocarbons. *Photochem. Photobiol.* **1999**, *70*, 10−34.

(3) Tielens, A. G. G. M. *The Physics & Chemistry of the Interstellar Medium*; Cambridge University Press: New York, 2005.

(4) Draine, B. T. Photoelectric heating of Interstellar gas. *Astrophys. J., Suppl. Ser.* **1978**, *36*, 595−619.

(5) Tielens, A. G. G. M. Interstellar polycyclic aromatic hydrocarbon molecules. *Annu. Rev. Astron. Astrophys.* **2008**, *46*, 289−337.

(6) Salama, F.; Allamandola, L. J. Is a pyrene-like molecular ion the cause of the 4,430-Å diffuse interstellar absorption band? *Nature* **1992**, *358*, 42−43.

(7) Salama, F.; Allamandola, L. J.; Tielens, A. G. G. M. Neutral and ionized polycyclic aromatic hydrocarbons, diffuse interstellar bands and the ultraviolet extinction curve. *J. Chem. Soc., Faraday Trans.* **1993**, *89*, 2277−2284.

(8) Szczepanski, J.; Vala, M. Laboratory evidence for ionized polycyclic aromatic hydrocarbons in the interstellar medium. *Nature* **1993**, *363*, 699−701.

(9) Parisel, O.; Berthier, G.; Ellinger, Y. New clues for ionized polycyclic aromatic hydrocarbons as possible carriers of diffuse interstellar bands. *Astron. Astrophys.* **1992**, *266*, L1−L4.

(10) Yastrebov, S. G.; Ivanov-Omskiĭ, V. I. Optical Properties of Interstellar Medium. *Technol. Phys. Lett.* **2005**, *31*, 878−880.

(11) Micelotta, E. R. PAH processing in space. Ph.D. Dissertation, Leiden Observatory, Faculty of Science, Leiden University, Leiden, The Netherlands, 2009.

(12) Yu, H. Environmental carcinogenic polycyclic aromatic hydrocarbons: Photochemistry and phototoxicity. *J. Environ. Sci. Health, Part C: Environ. Carcinog. Ecotoxicol. Rev.* **2002**, *20*, 149−183.

(13) Dong, S.; Hwang, H.-M.; Harrison, C.; Holloway, L.; Shi, X.; Yu, H. UVA light-induced DNA cleavage by selected polycyclic aromatic hydrocarbons. *Bull. Environ. Contam. Toxicol.* **2000**, *64*, 467−474.

(14) Chen, S.; Lu, H.; Huang, C. Polyfluorenes for device applications. *Adv. Polym. Sci.* **2008**, *212*, 49−84.

(15) Jochims, H. W.; Rühl, E.; Baumgärtel, H.; Tobita, S.; Leach, S. VUV peaks in absorption spectra and photoion yield curves of polycyclic aromatic hydrocarbons and related compounds. *Int. J. Mass Spectrom. Ion Processes* **1997**, *167/168*, 35−53.

(16) Jochims, H. W.; Baumgärtel, H.; Leach, S. Structure-dependent photostability of polycyclic aromatic hydrocarbon cations: Laboratory studies and astrophysical implications. *Astrophys. J.* **1999**, *512*, 500−510.

(17) Boschi, R.; Clar, E.; Schmidt, W. Photoelectron spectra of polynuclear aromatics. III. The effect of nonplanarity in sterically overcrowded aromatic hydrocarbons. *J. Chem. Phys.* **1974**, *60*, 4406−4418.

(18) Schmidt, W. Photoelectron spectra of polynuclear aromatics. V. Correlations with ultraviolet absorption spectra in the catacondensed series. *J. Chem. Phys.* **1977**, *66*, 828−845.

(19) Klasinc, L. Photoelectron spectra of conjugated molecules. *Pure Appl. Chem.* **1980**, *52*, 1509−1524.

(20) Deleuze, M. S. Valence one-electron and shake-up ionization bands of polycyclic aromatic hydrocarbons. II. Azulene, phenanthrene, pyrene, chrysene, triphenylene, and perylene. *J. Chem. Phys.* **2002**, *116*, 7012−7026.

(21) Schirmer, J.; Cederbaum, L. S.; Domcke, W.; Von Niessen, W. Strong correlation effects in inner-valence ionization of N_2 and CO. *Chem. Phys.* **1977**, *26*, 149−153.

(22) Cederbaum, L. S.; Schirmer, J.; Domcke, W.; Von Niessen, W. Complete breakdown of the quasiparticle picture for inner valence electrons. *J. Phys. B: At., Mol. Opt. Phys.* **1977**, *10*, L549−L553.

(23) Cederbaum, L. S.; Domcke, W. Theoretical aspects of ionization potentials and photoelectron spectroscopy: A Green's function approach. In *Advances in Chemical Physics*; Prigogine, I., and Rice, S. A., Eds.; Wiley: New York, 1977; Vol. *36*.

(24) Cederbaum, L. S.; Domcke, W.; Schirmer, J.; Von Niessen, W.; Diercksen, G. H. F.; Kraemer, W. P. Correlation effects in the ionization of hydrocarbons. *J. Chem. Phys.* **1978**, *69*, 1591−1603.

(25) Von Niessen, W. Application of a Green's function method to calculation of photoelectron spectra. *Bull. Soc. Catal. Cièn.* **1991**, *11*, 227−262.

(26) Plekan, O.; Coreno, M.; Feyer, V.; Moise, A.; Richter, R.; de Simone, M.; Sankari, R.; Prince, K. C. Electronic state resolved PEPICO spectroscopy of pyrimidine. *Phys. Scr.* **2008**, *78*, 058105.

(27) Fahlman, A.; Krause, M. O.; Carlson, T. A.; Svensson, A. Xe 5s,5p correlation satellites in the region of strong interchannel interactions, 28−75 eV. *Phys. Rev. A* **1984**, *30*, 812−819.

(28) Kutzner, M.; Radojević, V.; Kelly, H. P. Extended photoionization calculations for xenon. *Phys. Rev. A* **1989**, *40*, 5052−5057.

(29) Kivimäki, A.; Pfeiffer, L.; Aksela, H.; Nõmmiste, E.; Aksela, S. Intensities of the xenon $N_{4,5}OO$ Auger electron spectrum revisited. *J. Electron Spectrosc. Relat. Phenom.* **1999**, *101*, 43−47.

(30) Jaffe, H. H. *Symmetry in Chemistry.*; Wiley: New York, 1967.

(31) Parr, R. G.; Yang, W. *Density functional theory of atoms and molecules*; Oxford University Press: New York, 1989.

(32) Dreizler, R. M.; Gross, E. K. U. *Density functional theory*; Springer-Verlag: Berlin, 1990.

(33) Koch, W.; Holthausen, M. *A Chemist's Guide to Density Functional Theory*, 2nd ed.; Wiley-VCH: Weinheim, Germany, 2001.

(34) Becke, A. D. Density functional thermochemistry. III. The role of exact exchange. *J. Chem. Phys.* **1993**, *98*, 5648−5652.

(35) Lee, C.; Yang, W.; Parr, R. G. Development of the Colle-Salvetti correlation-energy formula into a functional of the electron density. *Phys. Rev. B* **1988**, *37*, 785−789.

(36) Dunning, T. H., Jr. Gaussian basis sets for use in correlated molecular calculations. I. The atoms boron through neon and hydrogen. *J. Chem. Phys.* **1989**, *90*, 1007−1023.

(37) Kendall, R. A.; Dunning, T. H.; Harrison, R. J. Electron affinities of the first-row atoms revisited. Systematic basis sets and wave functions. *J. Chem. Phys.* **1992**, *96*, 6796−6806.
(38) Frisch, M. J.; Trucks, G. W.; Schlegel, H. B.; Scuseria, G. E.; Robb, M. A.; Cheeseman, J. R.; Scalmani, G.; Barone, V.; Mennucci, B.; Petersson, G. A.; et al. *Gaussian 09*, revision B.01; Gaussian, Inc.: Wallingford, CT, 2009.
(39) Mayer, P. M.; Blanchet, V.; Joblin, C. Threshold photoelectron study of naphthalene, anthracene, pyrene, 1,2-dihydronaphthalene, and 9,10-dihydroanthracene. *J. Chem. Phys.* **2011**, *134*, 244312.
(40) Potts, A. W.; Holland, D. M. P.; Trofimov, A. B.; Schirmer, J.; Karlsson, L.; Siegbahn, K. An experimental and theoretical study of the valence shell photoelectron spectra of purine and pyrimidine molecules. *J. Phys. B: At., Mol. Opt. Phys.* **2003**, *36*, 3129−3143.
(41) Cederbaum, L. S.; Schirmer, J.; Domcke, W.; Von Niessen, W. On the adequacy of the molecular-orbital picture for describing ionization processes. *Int. J. Quantum Chem.* **1978**, *14*, 593−601.
(42) Cederbaum, L. S.; Domcke, W.; Schirmer, J.; Von Niessen, W. Many-Body Effects in Valence and Core Photoionization of Molecules. *Phys. Scr.* **1980**, *21*, 481−491.
(43) Carravetta, V.; Yang, L.; Ågren, H. Partial channel photoionization cross sections of polyenes. *Phys. Rev. B* **1997**, *55*, 10044−10050.
(44) Baltzer, P.; Karlsson, L.; Wannberg, B.; Öhrwell, G.; Holland, D. M. P.; MacDonald, M. A.; Hayes, M. A.; von Niessen, W. An experimental and theoretical study of the valence shell photoelectron spectrum of the benzene molecule. *Chem. Phys.* **1997**, *224*, 95−119.
(45) Korika, S.; Rolles, D.; Reinköster, A.; Langer, B.; Viefhaus, J.; Cvejanović, S.; Becker, U. Partial cross sections and angular distributions of resonant and nonresonant valence photoemission of C_{60}. *Phys. Rev. A* **2005**, *71*, 013203.
(46) Bertsch, G. F.; Bulgac, A.; Tamánek, D.; Wang, Y. Collective plasmon excitations in C_{60} clusters. *Phys. Rev. Lett.* **1991**, *67*, 2690−2693.
(47) Ling, Y.; Lifshitz, C. Plasmon excitation in polycyclic aromatic hydrocarbons studied by photoionization. *Chem. Phys. Lett.* **1996**, *257*, 587−591.
(48) Verkhovtsev, A. V.; Korol, A. V.; Solov'yov, A. V.; Bolognesi, P.; Ruocco, A.; Avaldi, L. Interplay of the volume and surface plasmons in the electron energy loss spectra of C_{60}. *J. Phys. B: At., Mol. Opt. Phys.* **2012**, *45*, 141002.
(49) Duley, W. W. A plasmon resonance in dehydrogenated coronene ($C_{24}H_x$) and its cations and the origin of the interstellar extinction band at 217.5 nm. *Astrophys. J. Lett.* **2006**, *639*, L59−L62.
(50) Carlson, T. A.; Gerard, P.; Krause, M. O.; Grimm, F. A.; Pullen, B. P. Photoelectron dynamics of the valence shells of benzene as a function of photon energy. *J. Chem. Phys.* **1987**, *86*, 6918−6926.
(51) Léger, A.; Verstraete, L.; d'Hendecourt, L.; Défourneau, D.; Dutuit, O.; Schmidt, W.; Lauer, J. C. The PAH hypothesis and the extinction curve. In *Interstellar Dust*; Allamandola, L. J., Tielens, A. G. G. M., Eds.; Kluwer: Dordrecht, The Netherlands, 1989; IAU Collect. Vol. *135*, pp 173−180.